HHS Public Access

Author manuscript

Adv Healthc Mater. Author manuscript; available in PMC 2021 January 01.

Published in final edited form as:

Adv Healthc Mater. 2020 January ; 9(1): e1901223. doi:10.1002/adhm.201901223.

Size-Dependent EPR Effect of Polymeric Nanoparticles on Tumor Targeting

Homan Kang, **Sunghoon Rho**, **Wesley R. Stiles**, **Shuang Hu**, **Yoonji Baek**, **Do Won Hwang**, **Satoshi Kashiwagi**

Gordon Center for Medical Imaging, Department of Radiology, Massachusetts General Hospital and Harvard Medical School, Boston, MA 02114 (United States)

Moon Suk Kim*,

Department of Molecular Science and Technology, Ajou University, Suwon, 16499, (South Korea)

Hak Soo Choi*

Gordon Center for Medical Imaging, Department of Radiology, Massachusetts General Hospital and Harvard Medical School, Boston, MA 02114 (United States)

Abstract

Passive targeting of large nanoparticles by the enhanced permeability and retention (EPR) effect is a crucial concept for solid tumor targeting in cancer nanomedicine. There is, however, a trade-off between the long-term blood circulation of nanoparticles and their nonspecific background tissue uptake. To define this size-dependent EPR effect, we designed near-infrared fluorophore-conjugated polyethylene glycols (PEG-ZW800s; 1–60 kDa) and evaluated their biodistribution, pharmacokinetics, and renal clearance in tumor-bearing mice. The targeting efficiency of size-variant PEG-ZW800s was investigated in terms of tumor-to-background ratio (TBR). Interestingly, smaller sized PEGs (≤20 kDa, 12 nm) exhibited significant tumor targeting with minimum to no nonspecific uptakes, while larger sized PEGs (>20 kDa, 13 nm) accumulated highly in major organs, including the lungs, liver, and pancreas. Among those tested, 20 kDa PEG-ZW800 exhibited the highest TBR, while excreting unbound molecules to the urinary bladder. This result lays a foundation for engineering tumor-targeted nanoparticles and therapeutics based on the size-dependent EPR effect.

Graphical Abstract

*To whom correspondence should be addressed: MSK at moonskim@ajou.ac.kr and HSC at hchoi12@mgh.harvard.edu.

Supporting Information

Supporting Information is available online from Wiley InterScience or from the author.

EPR-based passive tumor targeting of polymeric nanoparticles should consider the effect of molecular weight and hydrodynamic diameter on their biodistribution, pharmacokinetics, and renal clearance.

Keywords

Enhanced permeability and retention; Poly(ethylene glycol); Pharmacokinetics; Renal clearance; Tumor targeting

1. Introduction

Nanoparticles (NPs) hold great promise for bioimaging, disease diagnosis, and therapy in nanomedicine.[1] To utilize the advantages of NPs for specific targeting of organs/lesions, it is essential to understand the effect of physicochemical properties (*e.g.* size, shape, flexibility, surface charges, hydrophilicity/lipophilicity, and composition) of NPs on biodistribution, elimination, and targeting efficiency in biological systems.[2] For instance, zwitterionic NPs show rapid systemic circulation and low nonspecific uptake by the mononuclear phagocyte system (MPS), while positively charged NPs associate with serum protein, resulting in high uptake by the MPS.[3] In addition, size drives several biological phenomena with discrete cut-off size ranges, including circulation half-life, clearance pattern, extravasation through leaky vasculature, and macrophage uptake.[4] It is also well-known that the first and foremost requirement for designing a tumor-targeted NP is to make it large enough for long-term blood circulation to increase the chance of tumoral uptake and to avoid physical and biological barriers (*e.g.*, diffusion, aggregation, protein adsorption, phagocytic sequestration, and renal clearance).[5] However, rapid clearance either by renal or hepatic excretion can reduce the nonspecific background uptake of NPs in major organs which improves tumor-specific imaging and potential toxicity.[3b, 6] The precise control of these two contradictory phenomena stems from the understanding of pharmacokinetics (PK) and physicochemical properties of NPs. However, only a limited number of studies have been conducted to define the fundamental physicochemical properties of NPs that influence their circulation, biodistribution, clearance, and tumor targeting,[2a, 3b, 3c, 4a, 7] because most studies were focused on novel nanomaterials and rushed to publish proof-of-concept.[8] Consequently, the exact size of NPs that are required to avoid physiological biological barriers (*e.g.*, glomerular filtration or extravasation through blood fenestration) is still unclear and misunderstood, which has hampered the clinical translation of NPs.[5] For instance, NPs with a hydrodynamic diameter (HD) of 100–400 nm have previously been

considered optimal for passive tumor targeting due to the enhanced permeability and retention (EPR) effect; however, Cabral *et. al* has recently reported that 30 nm micelles could show much more effective tumor penetration than 100 nm micelles.[7d] Similarly, the glomerular filtration barrier is known as a 'size-cutoff' slit; however, the Zheng group recently discovered that this glomerular filtration acts as an atomically precise 'bandpass' barrier in sub-nanometer regimes.[7g] Here we report the size-dependent EPR effect of polymeric nanoparticles on tumor targeting using polyethylene glycol (PEG) in terms of their PK, biodistribution, and clearance. The outcome of this study provides a design consideration of NP-based therapeutics and nanomedicine with a better understanding of EPR-based passive tumor targeting as well as reducing potential toxicity by renal clearance.

2. Results

2.1 Preparation of PEG-ZW800s

PEG is commonly used to design biodegradable and biocompatible NPs or biologically active agents (proteins, peptides, enzymes, antibody fragments, oligonucleotides, small synthetic drugs, etc.). The repeated ethylene glycol units form tight associations with water molecules, resulting in the formation of a hydrating layer (Figure 1a).[9] PEGylation of bioactive agents has extensively been studied to increase the solubility of water-insoluble compounds, lower the toxicity of drugs, generate the desired PK profile, and enhance specific uptake at the target site. To monitor the *in vivo* behaviors of PEGs, near-infrared (NIR) fluorescent ZW800–1C[10] was conjugated to a series of monoamino- or diamino-PEGs (1–60 kDa) as depicted in Figure 1b and Figure S1. PEG-ZW800s were purified by membrane dialysis, and their purity was evaluated by size exclusion chromatography (>93%; Figure S2). In addition, PEG-ZW800s showed no significant difference in the absorbance and emission spectra when compared to those of ZW800–1C (Figure 1C). The HD of PEGs was determined using gel filtration chromatography with a standard calibration curve of HD size markers (ferritin; 440 kDa, 12.20 nm, ovalbumin; 44 kDa, 6.10 nm HD, ribonuclease; 13.7 kDa, 3.28 nm, and aprotinin; 6.5 kDa, 1.96 nm). As shown in Table 1, the HD of PEG increased proportionally with the molecular weight (MW) of PEG and showed a range from 1 to 19 nm.

2.1 Biodistribution and Pharmacokinetics of PEG-ZW800s

We investigated the biodistribution, renal clearance, and PK of six different sized PEG-ZW800s in CD-1 mice (Figure 2). Small-sized PEGs (1, 5, 10, and 20 kDa) initially distributed rapidly into the blood, liver, kidney, duodenum, and other major organs within 1 min post-injection, then the overall signal decreased from the major organs, while the signal in the kidneys increased over time due to active renal excretion. In the case of larger PEGs (40 and 60 kDa), the initial signal distribution was similar to the others, but stayed longer in the bloodstream (Figure 2a). In particular, PEG 60 kDa showed signals in the inferior vena cava and the left renal vein even 4 h post-injection. Since larger PEGs is difficult to extravasate, they resulted in high background signals in almost all central and peripheral tissues, including the heart, lungs, liver, pancreas, kidney, spleen, duodenum, and intestines (Figures 2b,c and Figure S3).

We summarized the relationship among MW, HD, and PK parameters of PEGs after a single intravenous injection in Table 1. Urine samples were collected at 4 h post-intravenous injection and the urinary excretion values (% injection dose; ID) of PEGs were calculated by measuring the NIR fluorescence signals in the urine (Figure S4). Urinary excretion showed a proportional decrease with the MW of PEGs (~85 %ID for 1 kDa to ~5 %ID for 60 kDa). This size-dependent renal clearance is consistent with the finding that smaller NPs are more efficiently cleared out through the urine than larger NPs.[3a, 4b, 7g, 11] Even though the size is over the glomerular filtration threshold (6–8 nm),[3–4] larger PEGs (>40 kDa) also show ~5%ID of urinary excretion values because of the randomly coiled linear structure of PEG.

Due to the restricted extravasation of larger-sized PEG-ZW800s, prolonged half-life values were observed (Figure 2d and Table 1). The elimination half-life of PEGs gradually increased from 24 min to 224 min as the MW of PEGs increased from 1 kDa to 60 kDa. More importantly, the area-under-the-curve (AUC) increased dramatically with the MW of PEGs (990, 1034, 3135, 3801, 10241, and 24806 %ID·g^{-1}·min for 1, 5, 10, 20, 40, and 60 kDa of PEGs, respectively) because macromolecules barely permeate the endothelium of normal blood vessels.[7f] The longer elimination half-life and larger AUC values are favorable for tumoral uptake because of the increased chance of reaching the tumor site.[4d] Tumors have functional defects in lymphatic vessels, and such decreased lymphatic drainage results in retention of permeated polymeric NPs in the tumor microenvironment.[12] Together, the HD of PEGylated molecules is the most dominant factor in biodistribution and PK,[3c] unlike small molecules where other surface properties are more prevailing (Figure 2e).[13] This effect can be seen in Figure S5, where the difference between biodistribution and PK of free ZW800–1C and PEGylated ZW800–1C is shown.

2.3 Passive Tumor Targeting Efficiency for Polymeric NPs

The polymer-based nanoplatforms such as polymeric assemblies,[14] liposomes,[15] and polymer-drug conjugates[16] can lead to high therapeutic concentrations of anticancer drugs to tumors by the EPR effect. However, for clinical translation, it is very important that these NPs should be non-toxic and eliminated from the body in a reasonable period of time.[17] In this context, we compared size-varying PEG-ZW800s with the effectiveness of tumor targeting in terms of tumor-to-background ratio (TBR) and potential toxicity in HeLa tumor-bearing mice (Figure 3). After a single intravenous injection, PEG-ZW800s appeared immediately in the bloodstream and distributed quickly to the peripheral compartments, followed by gradual excretion (see Supplementary Movie S1). As shown in Figure 3a, smaller PEGs (≤20 kDa, 11 nm) were mainly excreted to the bladder after 1 h injection. In the meantime, tumor signals from the mice injected with 10 kDa and 20 kDa PEGs were clearly distinguished from the background signal (Figure 3b; TBR = 3.7 and 4.4 for PEG 10 kDa and 20 kDa, respectively). In contrast, larger PEGs (≥40 kDa, 13 nm) distributed almost everywhere in the body even 24 h post-injection. The signals in the tumor site increased; however, background signals remained high, resulting in relatively low TBR values (Figure 3b, absolute fluorescence intensities are provided in Figure S6). TBR at 24 h and integration of TBR vs. MW are shown in Figure 3c (also shown in Figure S7 for *ex vivo* TBR data). Consequently, 20 kDa PEG (11 nm) showed the best performance in terms of TBR: signal remained in the tumor while nonspecific background signals were minimized.

2.4 Passive Tumor Targeting Efficiency vs. Renal Clearance

NPs administered in the body follow either a renal or hepatobiliary excretion pathway.[18] Renal excretion is preferred for NPs because it reduces potential toxicity thus increasing clinical utility. Renal clearable NPs excrete rapidly from the body while little cellular internalization and metabolism are involved, thus effectively minimizing biological and immunological exposure.[17] Thus, smaller size and hydrophilic NPs in particular can avoid undergoing sequestration by the MPS in the spleen, lymph nodes, and liver. Figure 4a displays PK values of size-varying PEGs in terms of AUC vs. renal excretion: AUC correlated with the HD of PEGs, while renal excretion decreases exponentially as HD increased. Figure 4b illustrates the size effect on renal clearance and EPR. Supposing that the administrated NPs are in equilibrium with the central compartment and the peripheral compartments, it is desirable that NPs are excreted from the body while retaining tumor signal by the EPR effect. When NPs are excreted by the liver and/or kidneys, the overall concentrations decrease in the central and peripheral compartments through the equilibrium among each compartment.

3. Discussion

In study, we have demonstrated the size-dependent EPR of PEG-ZW800s in terms of their blood circulation, biodistribution, renal clearance, and tumor targeting. Researchers have also studied these parameters using proteins, PEG polymers, and other copolymers.[7f, 7h, 7i, 19] For example, Matsumura *et al.* reported that an increase in MW of a protein prolongs its plasma half-life, which in turn leads to higher passive tumor distribution.[19] Similarly, Seymour *et al.* demonstrated that large copolymers (MW >40 kDa) are unable to be excreted via the kidney filter and urinary track, and thus persist in circulation, whereas smaller copolymers (MW <40 kDa) are subject to rapid renal clearance.[7h] Clearly, it is not disputed that the molecular size of an NP governs its *in vivo* transport and nano-bio interactions, however, the optimal size has yet to be agreed upon.

In addition, in the case of smaller PEGs (<5 kDa), we need to further investigate their nano-bio interactions because the physicochemical properties of conjugated fluorophores may affect the overall fate of small PEGylated compounds. For instance, PEG-ZW800 (1 kDa) is composed of PEG (MW = 1 kDa) and ZW800–1C (MW = 928 Da), of which the molecular behavior is found to be similar to the free dye (Figures 2,S5) because the physicochemical property of ZW800–1C may strongly affect the biodistribution and PK of PEG conjugates. However, when PEG chains are longer than 5 kDa, the effect of conjugated dyes on the biodistribution and/or tumoral uptake should be minimal, resulting in size-dependent blood circulation and renal clearance (Figures 3,4).

Although previous studies have been focused on the MW, this information is insufficient in determining the cut-off size ranges of NPs in living organisms. Instead, the HD of an NP is more important in predicting its biological activity, since nanomaterials including polymers and proteins assume different 3D conformations such as globular, linear, cylindrical, and dendritic structures. In addition, hybrid NPs with the same MW may have largely different HDs depending on their surface charges, shape, compositions, rigidity/flexibility, hydrophilicity/lipophilicity, etc.[18] Therefore, such physicochemical properties of an NP

should be considered as a standard feature when investigating biological/physiological phenomena with discrete cut-off size ranges.

The size effect of polymeric NPs on tumor targetability has also been extensively studied.[7f, 7h, 7i] Previously many groups have found that larger sized NPs are better for tumor targeting, however, this statement is incomplete in that it only considers tumor accumulation index without off-target distribution in normal tissues, organs, and blood.[7i] One of the significant issues in the clinical translation is such potential off-target toxicity caused by nonspecific uptake. A trade-off arises between "size increase/higher tumor targeting/low clearance rate/high background" *vs* "size decrease/lower tumor targeting/high clearance rate/less background." Increase in the size of a NP prolongs systemic blood circulation and thus EPR-based targeting. At the same time, however, background signal/nonspecific uptake could increase proportionally. Therefore, simply increasing the size cannot guarantee higher image contrast at the target tissue. On the other hand, decreasing the size sacrifices the area under the plasma concentration versus time curve, resulting in faster background clearance but lower targeting efficiency. It is important to consider all factors when determining the optimal size required to avoid biological barriers and toxicity. In this study, equal importance has been given to size effects and off-target distribution to determine the optimal PEG size that results in a balance of targeting and clearance in tumor imaging.

Although many PEGylated compounds have been approved by the FDA for clinical use via injection, topical, rectal, and nasal administration, PEG is not the only hydrophilic molecule that improves tumor targetability.[9] Many researchers utilize supramolecular self-assembling structures like micelles that generate NPs larger than 10 nm in HD. Although these NPs have excessive functionality, the large HD can cause potential off-target toxicity through the nonspecific uptake caused by the MPS (*a.k.a.*, reticuloendothelial system; RES). As we began to better understand the interaction between a NP and kidney filtration at the molecular level, several NPs have been engineered to be small in size (renal clearable) which reduces potential toxicity and improves biocompatibility.[3] Examples of smaller NP vehicles include H-Dots (HD <5.5 nm) for image-guided drug delivery,[3c] ultrasmall gold NPs (HD <5 nm) for tumor targeting,[20] polymer surfactant-encapsulated nanocomplexes (HD <10 nm) as a delivery system with high blood-brain barrier permeability,[21] and ultrasmall inorganic hybrid NPs (HD ~6 nm) for optical-PET imaging.[22]

4. Conclusions

We found that small-sized polymeric NPs (<12 nm) can target tumor sites by the EPR effect, and renal clearance of administrated NPs enhances TBR and reduces potential toxicity. As the MW of PEGs increase from 1 kDa to 60 kDa, the elimination half-life (24.37 to 224.14 min) and AUC values (990 to 24,806 %ID·g^{-1}·min) increased proportionally. PEGs smaller than 12 nm showed minimal nonspecific uptake, while larger PEGs accumulated in major organs such as the lungs, liver, and pancreas with prolonged systemic circulation. Even small sized PEGs with MW of 5 kDa exhibited reasonable uptake in the tumor site *via* the EPR effect, and 20 kDa PEG with 11 nm in HD showed the best performance and maximized TBR with rapid renal excretion. This study lays a foundation for designing NP-

based therapeutics and nanomedicine with a better understanding of EPR-based passive tumor targeting and the importance of reducing potential toxicity by renal clearance.

5. Experimental Section

Materials:

Poly(ethylene glycol), 1,1'-Carbonyldiimidazole, ethylenediamine, dipyrrolidino(N-succinimidyloxy)carbenium hexafluorophosphate (HSPyU), bovine serum albumin (BSA), *N,N*-diisopropylethylamine (DIEA), acetone, tetrahydrofuran, dimethyl sulfoxide (DMSO) and ethanol were purchased from Fisher Scientific (Pittsburgh, PA), Sigma-Aldrich (Saint Louis, MO), or Acros Organics (Morris Plains, NJ).

Synthesis of PEGylated NIR Fluorophores:

Linear monoamino-PEG (1 kDa) or diamino-PEGs (5, 10, 20, 40, and 60 kDa) were conjugated with ZW800–1C to yield PEG-ZW800s with varying lengths from 2–16 nm. To form the *N*-hydroxysuccinimide (NHS)-activated ester, ZW800–1C (100 mg, 0.1 mmol) was dissolved in 50 mL of anhydrous DMSO. Then, 0.1 mL of DIEA and HSPyU (82 mg, 2 mmol) were added to the solution. After stirring for 2 h at room temperature, the reaction mixture was poured into 250 mL of acetone/ethanol (1:1 *v/v*). The precipitate was filtered and washed with acetone/ethanol several times to remove excess reagent. The resulting ZW800–1C NHS ester was dried overnight *in vacuo*. For conjugation, ZW800–1C-NHS ester (50 μmol) was added to amino-PEGs (25 μmol) in 5 mL of PBS (pH 8.0). The reaction mixture was stirred for 12 h, then excess reagents were removed by membrane dialysis (3500 kDa MWCO). The resultants were lyophilized to yield the desired PEG-ZW800.

The purity of all compounds was measured using size-exclusion chromatography (SEC) analysis on the Agilent HPLC system consisting of a 1260 binary pump with a 1260 ALS injector, a 35900E Photodiode Array detector (Agilent, 200–800 nm), and a 2475 multi-wavelength fluorescence detector (Waters, Ex 770 nm and Em 790 nm). A portion of the eluent flowed into the PDA equipped with an Ultrahydrogel 2000 (7.8 × 300 mm) SEC column. The mobile phase was 0.1% formic acid in water for 30 min with a flow rate of 0.75 mL/min.

Fluorescence Imaging:

Mice were imaged using the in-house built real-time intraoperative NIR imaging system. A 760-nm excitation laser source (4 mW/cm) was used with white light (400–650 nm; 40,000 lux). Color and NIR fluorescence images were acquired simultaneously with customized software at rates of up to 15 Hz over a field of view with 15 cm in diameter.

Animal Model and Experiment:

Animals were housed in an AAALAC-certified facility staffed by full-time veterinarians and were studied under the supervision of MGH IACUC in accordance with the approved institutional protocol (N2016000529). 6-week-old CD-1 male mice were purchased from Charles Laboratories (Wilmington, MA). All animals acclimated to the animal facility for at least 48 h prior to experimentation. Exposure to isoflurane inhalant anesthesia was used to

anesthetize mice for brief non-surgical procedures. To establish tumor-xenografted nude mice, HeLa cells were cultured in DMEM with 5% FBS and 100 units/ml of penicillin and streptomycin. NCr nu/nu mice (Taconic Farms, Germantown, NY) were inoculated by subcutaneous injection with 2×10^6 HeLa cells suspended in 150 μL of 50% (*v/v*) saline/matrigel at the right flank. PEGs in 5% (*w/v*) BSA/saline (100 μM) were administered intravenously at a dose of 100 μL injection solution.

Biodistribution and Pharmacokinetics:

Mice were maintained under anesthesia by inhalation of isoflurane for the entire duration of the experiment. The end of the tail was cut to enable blood extraction. Before injection, blood was then sampled in heparinized capillary tubes (Fisher Scientific, Pittsburgh, PA) as a reference and collected blood was stored in an ice box to prevent clotting. Mice were injected with 25 nmol of each PEG-ZW800 and blood was collected at the following time points (1, 3, 5, 10, 30, 60, 120, 180, and 240 min) to estimate PK values including distribution ($t_{1/2\alpha}$) and elimination ($t_{1/2\beta}$) blood half-lives, plasma clearance and volume of distribution. After 4 h, mice were sacrificed to image organs and to collect urine from the bladder. At least 3 mice were analyzed for each sample. The collected blood samples were centrifuged for 20 min at 3000 rpm to separate serum and blood plasma, and supernatants were then filled into capillary tubes. Fluorescence intensities of the microtubes were measured using the in-house built NIR imaging system. Results were presented as a bi-exponential decay curve using Prism software (GraphPad, San Diego, CA).

Statistical and Quantitative Analyses:

All data depict the mean ± SEM with a minimum of 3 biological replicates. The fluorescence and background intensities of a region of interest over each tissue were quantified using customized imaging software and ImageJ v1.51j8 (National Institutes of Health, Bethesda, MD). The (tumor) signal-to-background ratio (SBR or TBR) was calculated as SBR = fluorescence signal in region of interest/background signal, where the background is the fluorescence intensity of muscle.

Supplementary Material

Refer to Web version on PubMed Central for supplementary material.

Acknowledgements

This study was supported by the following NIH grants: #R01EB022230, #R01HL143020, and #R21CA223270. This work was also supported by the Creative Materials Discovery Program through the National Research Foundation of Korea (2019M3D1A1078938). The content expressed is solely the responsibility of the authors and do not necessarily represent the official views of the NIH.

REFERENCES:

[1]. Markovsky E, Baabur-Cohen H, Eldar-Boock A, Omer L, Tiram G, Ferber S, Ofek P, Polyak D, Scomparin A, Satchi-Fainaro R, J. Controlled Release 2012, 161, 446–460.

[2]. a) Sykes EA, Chen J, Zheng G, Chan WC, ACS Nano 2014, 8, 5696–5706; [PubMed: 24821383] b) Kang H, Hu S, Cho MH, Hong SH, Choi Y, Choi HS, Nano Today 2018, 23, 59–72. [PubMed: 31186672]

[3]. a) Choi HS, Liu W, Misra P, Tanaka E, Zimmer JP, Itty Ipe B, Bawendi MG, Frangioni JV, Nat Biotechnol 2007, 25, 1165–1170; [PubMed: 17891134] b) Choi HS, Liu W, Liu F, Nasr K, Misra P, Bawendi MG, Frangioni JV, Nat Nanotechnol 2010, 5, 42–47; [PubMed: 19893516] c) Kang H, Gravier J, Bao K, Wada H, Lee JH, Baek Y, Fakhri G. El, Gioux S, Rubin BP, Coll JL, Choi HS, Adv. Mater 2016, 28, 8162–8168. [PubMed: 27414255]

[4]. a) Blanco E, Shen H, Ferrari M, Nat. Biotechnol 2015, 33, 941–951; [PubMed: 26348965] b) Choi HS, Ipe BI, Misra P, Lee JH, Bawendi MG, Frangioni JV, Nano Lett. 2009, 9, 2354–2359; [PubMed: 19422261] c) Zhou C, Long M, Qin Y, Sun X, Zheng J, Angewandte Chemie 2011, 50, 3168–3172; [PubMed: 21374769] d) Yu M, Zheng J, ACS Nano 2015, 9, 6655–6674. [PubMed: 26149184]

[5]. Wilhelm S, Tavares AJ, Dai Q, Ohta S, Audet J, Dvorak HF, Chan WC, Nature Reviews Materials 2016, 1, 16014.

[6]. Kang H, Han M, Xue J, Baek Y, Chang J, Hu S, Nam H, Jo MJ, Fakhri GE, Hutchens MP, Choi HS, Kim J, Nat. Commun 2019, 10, 5134. [PubMed: 31723130]

[7]. a) Yamaoka T, Tabata Y, Ikada Y, J Pharm Sci-Us 1994, 83, 601–606;b) Perrault SD, Walkey C, Jennings T, Fischer HC, Chan WC, Nano Lett. 2009, 9, 1909–1915; [PubMed: 19344179] c) He C, Hu Y, Yin L, Tang C, Yin C, Biomaterials 2010, 31, 3657–3666; [PubMed: 20138662] d) Cabral H, Matsumoto Y, Mizuno K, Chen Q, Murakami M, Kimura M, Terada Y, Kano M, Miyazono K, Uesaka M, Nat. Nanotechnol 2011, 6, 815–823; [PubMed: 22020122] e) Hirn S, Semmler-Behnke M, Schleh C, Wenk A, Lipka J, Schäffler M, Takenaka S, Möller W, Schmid G, Simon U, European journal of pharmaceutics and biopharmaceutics 2011, 77, 407–416; [PubMed: 21195759] f) Singh Y, Gao D, Gu Z, Li S, Stein S, Sinko PJ, Mol. Pharm 2012, 9, 144–155; [PubMed: 22077582] g) Du B, Jiang X, Das A, Zhou Q, Yu M, Jin R, Zheng J, Nat. Nanotechnol 2017, 12, 1096–1102; [PubMed: 28892099] h) Seymour L, Miyamoto Y, Maeda H, Brereton M, Strohalm J, Ulbrich K, Duncan R, European Journal of Cancer 1995, 31, 766–770;i) Lammers T, Kuhnlein R, Kissel M, Subr V, Etrych T, Pola R, Pechar M, Ulbrich K, Storm G, Huber P, Peschke P, Journal of controlled release : official journal of the Controlled Release Society 2005, 110, 103–118. [PubMed: 16274831]

[8]. Albanese A, Tang PS, Chan WC, Annu. Rev. Biomed. Eng 2012, 14, 1–16. [PubMed: 22524388]

[9]. Harris JM, Chess RB, Nat. Rev. Drug Discovery 2003, 2, 214–221. [PubMed: 12612647]

[10]. Hyun H, Owens EA, Narayana L, Wada H, Gravier J, Bao K, Frangioni JV, Choi HS, Henary M, RSC Adv. 2014, 4, 58762–58768. [PubMed: 25530846]

[11]. Choi HS, Ashitate Y, Lee JH, Kim SH, Matsui A, Insin N, Bawendi MG, Semmler-Behnke M, Frangioni JV, Tsuda A, Nat. Biotechnol 2010, 28, 1300–1303. [PubMed: 21057497]

[12]. Danquah MK, Zhang XA, Mahato RI, Adv Drug Deliv Rev 2011, 63, 623–639. [PubMed: 21144874]

[13]. Koo H, Lee JH, Bao K, Wu Y, El Fakhri G, Henary M, Yun SH, Choi HS, Adv. Healthc. Mater 2016, 5, 2510–2516. [PubMed: 27568818]

[14]. Gao GH, Li Y, Lee DS, J. Controlled Release 2013, 169, 180–184.

[15]. Allen TM, Cullis PR, Adv. Drug Delivery Rev 2013, 65, 36–48.

[16]. Kopeček J, Adv. Drug Delivery Rev 2013, 65, 49–59.

[17]. Kang H, Mintri S, Menon AV, Lee HY, Choi HS, Kim J, Nanoscale 2015, 7, 18848–18862. [PubMed: 26528835]

[18]. Choi HS, Frangioni JV, Mol Imaging 2010, 9, 291–310. [PubMed: 21084027]

[19]. Matsumura Y, Maeda H, Cancer Res. 1986, 46, 6387–6392. [PubMed: 2946403]

[20]. a) Peng C, Xu J, Yu M, Ning X, Huang Y, Du B, Hernandez E, Kapur P, Hsieh JT, Zheng J, Angew. Chem. Int. Ed 2019, 58, 8479–8483;b) Peng C, Yu M, Hsieh JT, Kapur P, Zheng J, Angewandte Chemie 2019, 58, 12076–12080. [PubMed: 31278873]

[21]. Park J, Choi E, Shin S, Lim S, Kim D, Baek S, Lee KP, Lee JJ, Lee BH, Kim B, Jeong K, Baik JH, Kim YK, Kim S, Journal of controlled release : official journal of the Controlled Release Society 2018, 284, 152–159. [PubMed: 29913220]

[22]. a) Phillips E, Penate-Medina O, Zanzonico PB, Carvajal RD, Mohan P, Ye Y, Humm J, Gonen M, Kalaigian H, Schoder H, Strauss HW, Larson SM, Wiesner U, Bradbury MS, Sci. Transl. Med 2014, 6, 260ra149;b) Kim SE, Zhang L, Ma K, Riegman M, Chen F, Ingold I, Conrad M, Turker

MZ, Gao M, Jiang X, Monette S, Pauliah M, Gonen M, Zanzonico P, Quinn T, Wiesner U, Bradbury MS, Overholtzer M, Nature nanotechnology 2016, 11, 977–985.

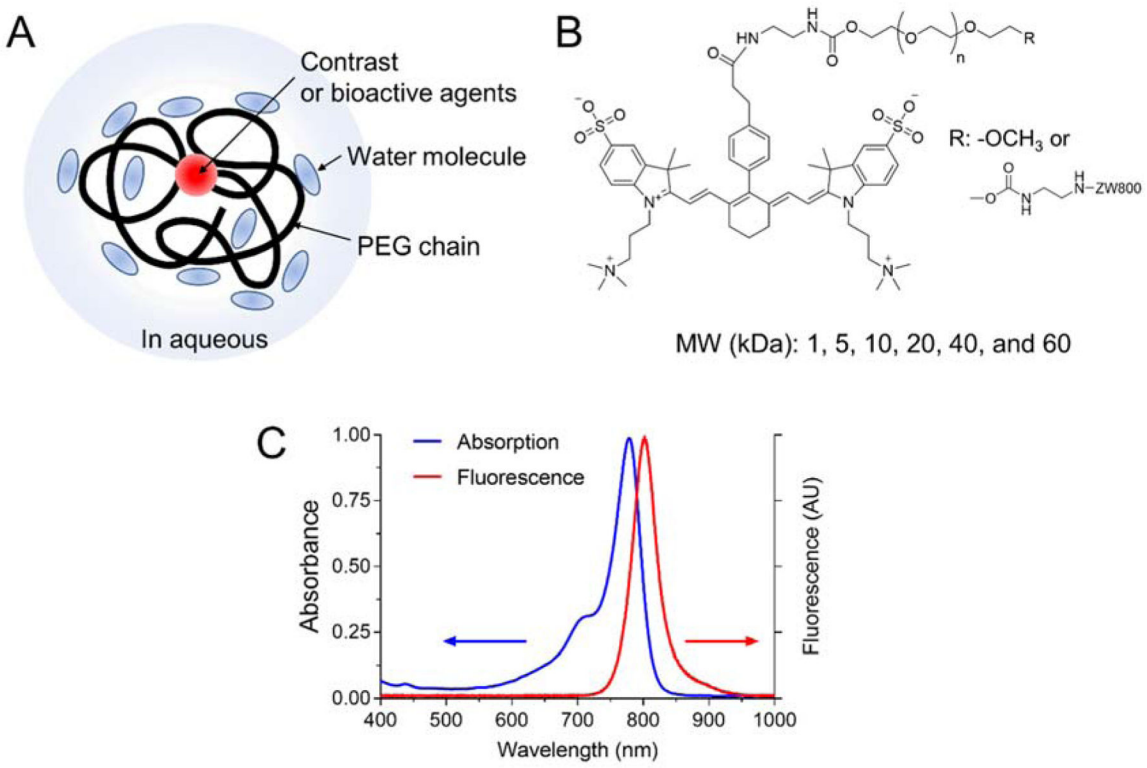

Figure 1.

Structural characteristics of PEGylated fluorophores and their optical properties. A) Schematic diagram and B) chemical structure and of PEG-ZW800. C) Representative absorption and fluorescence spectra of PEG-ZW800.

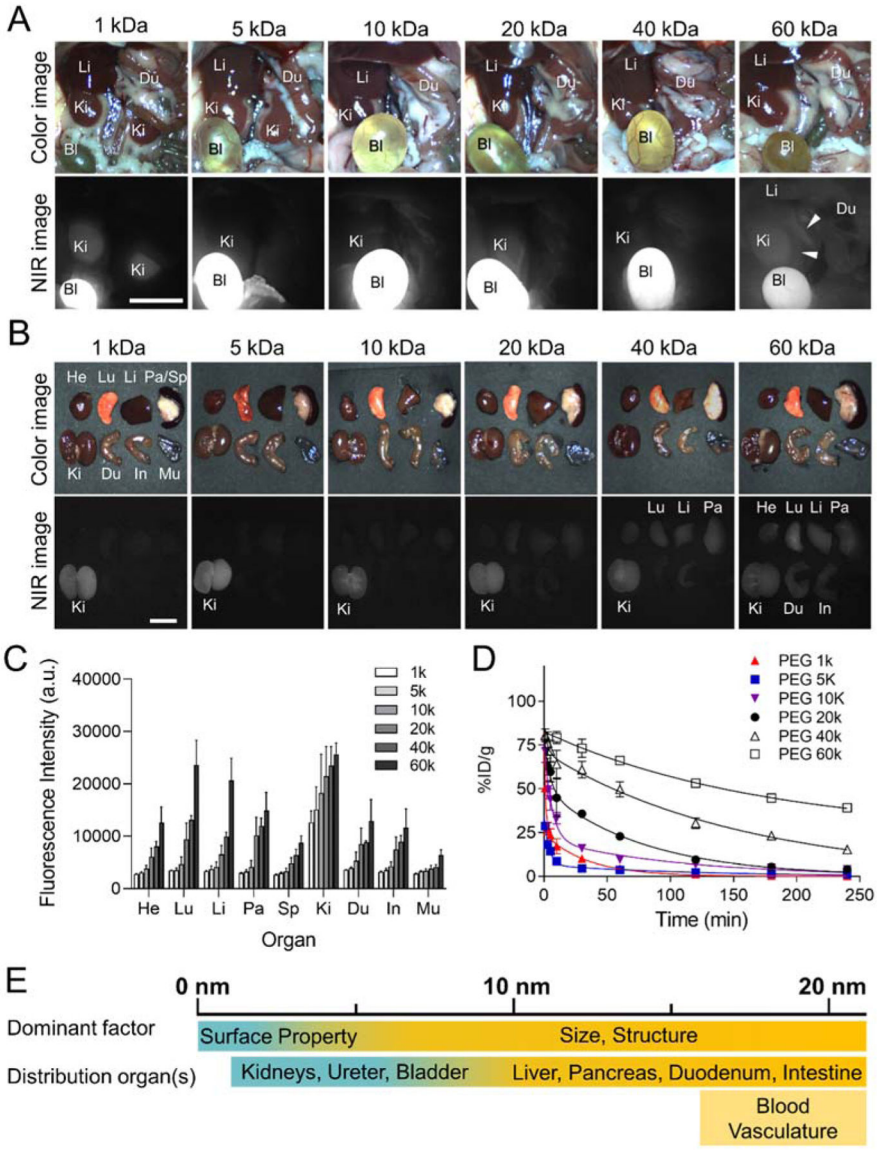

Figure 2.

In vivo biodistribution and PK of PEG-ZW800s with various MWs (1, 5, 10, 20, 40 and 60 kDa from left to right). 25 nmol of each agent was injected intravenously into CD-1 mice, and their NIR fluorescence images of A) abdominal cavity and B) resected organs were taken at 4 h post-injection. White arrowheads in (A) indicate the inferior vena cava and the left renal vein. Exposure time, 25 ms; scale bar, 1 cm. C) Fluorescence intensities of each organ. Abbreviations used are: Bl, bladder; Du, duodenum; He, heart; In, intestine; Ki, kidneys; Li, liver; Lu, lungs; Mu, muscle; Pa, pancreas; Sp, spleen; Mu, muscle (n=3–5, mean ± SEM). D) Blood concentration (%ID·g^{-1}) decay of PEG-ZW800s. E) Dominant factors in biodistribution and PK for polymeric NPs, including size, surface property, and structure.

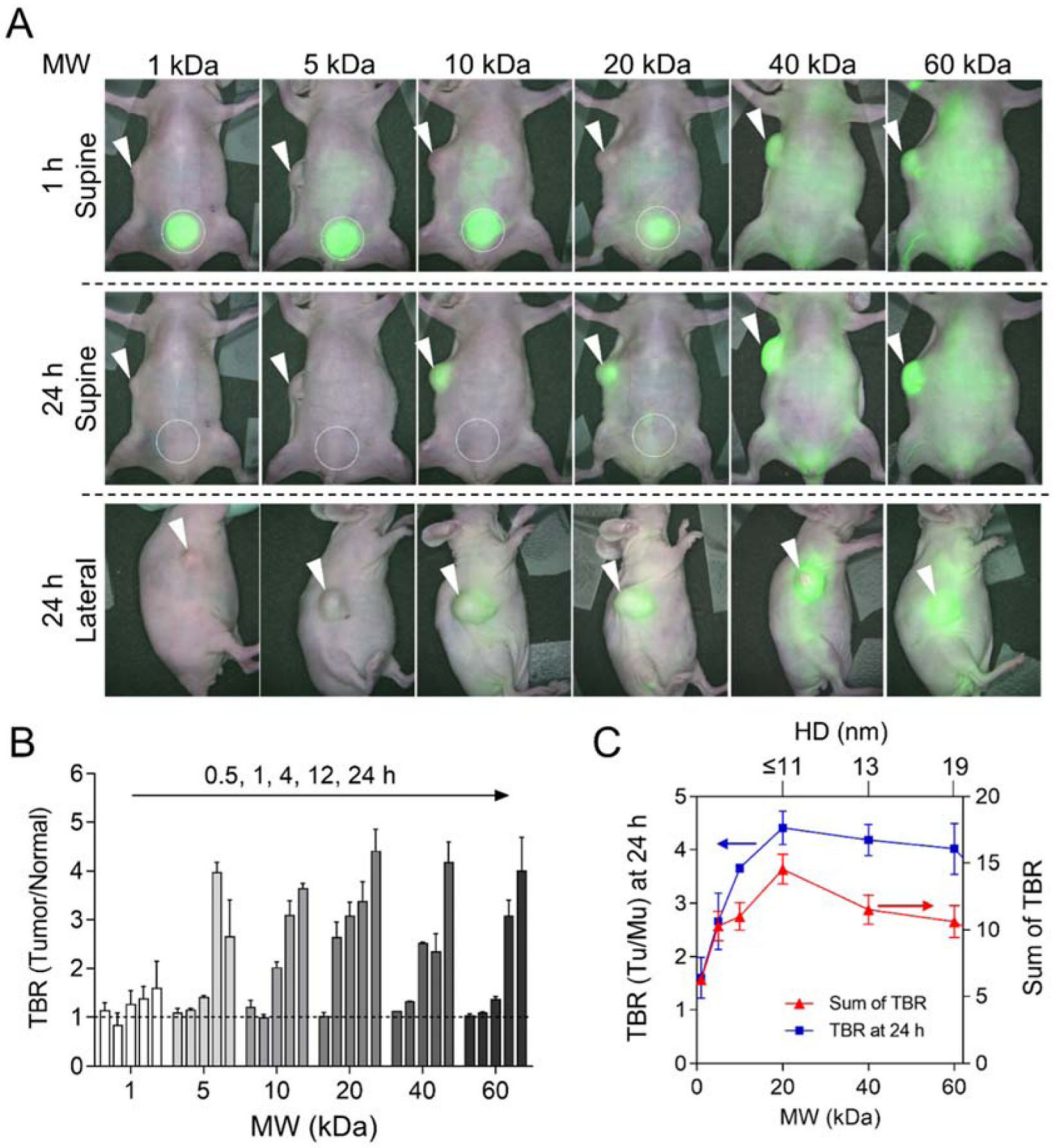

Figure 3.

Passive tumor targeting efficiency of PEG-ZW800s. A) PEG-ZW800 (25 nmol) was injected intravenously into HeLa xenograft mice, and the TBRs (tumor/muscle) were measured for 24 h post-injection. White arrowheads indicate tumor sites, and white circles indicate urinary excretion to bladders. B) TBR was measured in xenograft mice shown in (A) at 0.5, 1, 4, 12, and 24 h post-injection (left to right) (n = 3, mean ± SEM). C) The relationship between TBR and MW at 24 h post-injection. The axis for HD size is not to scale.

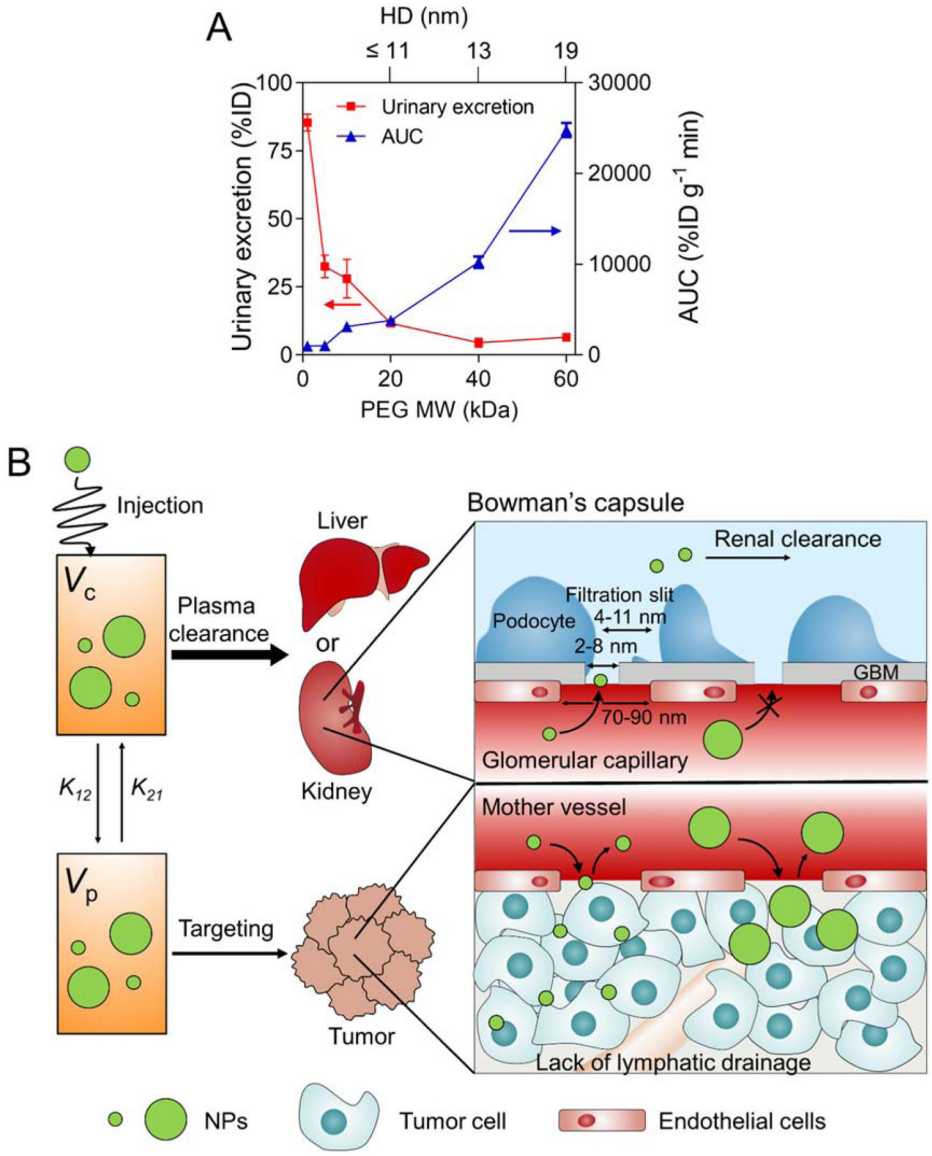

Figure 4.

The tradeoff between passive tumor targeting and systemic clearance. A) Correlation of renal excretion and area under the curve (AUC) values with the MW of PEG-ZW800s (n = 5, mean ± SEM). B) Illustration of size effect on renal clearance and passive tumor targeting efficiency via EPR effect.

Table 1.

Molecular weight, hydrodynamic diameter (HD) and pharmacokinetic (PK) parameters for various sizes of PEG-ZW800s

	PEG 1 kDa	PEG 5 kDa	PEG 10 kDa	PEG 20 kDa	PEG 40 kDa	PEG 60 kDa
MW (g mol^{-1})	~2000	~5000	~11000	~20000	~40000	~60000
HD (nm)[a]	1.0	2.9	6.9	10.9	13.0	18.8
$T_{½}$ α (min)[b]	0.83±0.07	3.15±0.74	5.19±3.32	13.65±6.84	-	-
$T_{½}$ β (min)	24.37±1.58	80.84±6.35	92.15±54.00	103.14±11.92	106.0±25.24	224.14±26.39
Urinary excretion (%ID)	85.4±5.4	32.6±7.2	28.0±12.4	11.6±1.4	4.5±2.8	6.5±1.5
AUC (%ID·g^{-1}·min)	990±304	1,034±198	3,135±435	3,801±733	10,241±1,101	24,806±1,343
Clearance (mL min^{-1})	0.111±0.034	0.101±0.022	0.033±0.005	0.027±0.005	0.010±0.001	0.004±0.0002
V_d (mL)	4.00±1.46	6.65±4.43	3.96±2.06	6.15±4.70	1.62±0.25	1.28±0.09

[a] HD values were measured by gel filtration chromatography using HD size markers: ferritin; 440 kDa, 12.2 nm, ovalbumin; 44 kDa, 6.10 nm HD, ribonuclease; 13.7 kDa, 3.28 nm and aprotinin; 6.5 kDa, 1.96 nm.

[b] $T_{½}$α values for PEG-ZW800 40 kDa and 60 kDa were not obtained due to the use of one-compartment model pharmacokinetics.

$t_{½}$α, distribution half-life; $t_{½}$β, elimination half-life; AUC, area under the curve; V_d, volume of distribution at elimination state. The time point for urinary excretion is 4 h post-injection